LA-12274

c. 3

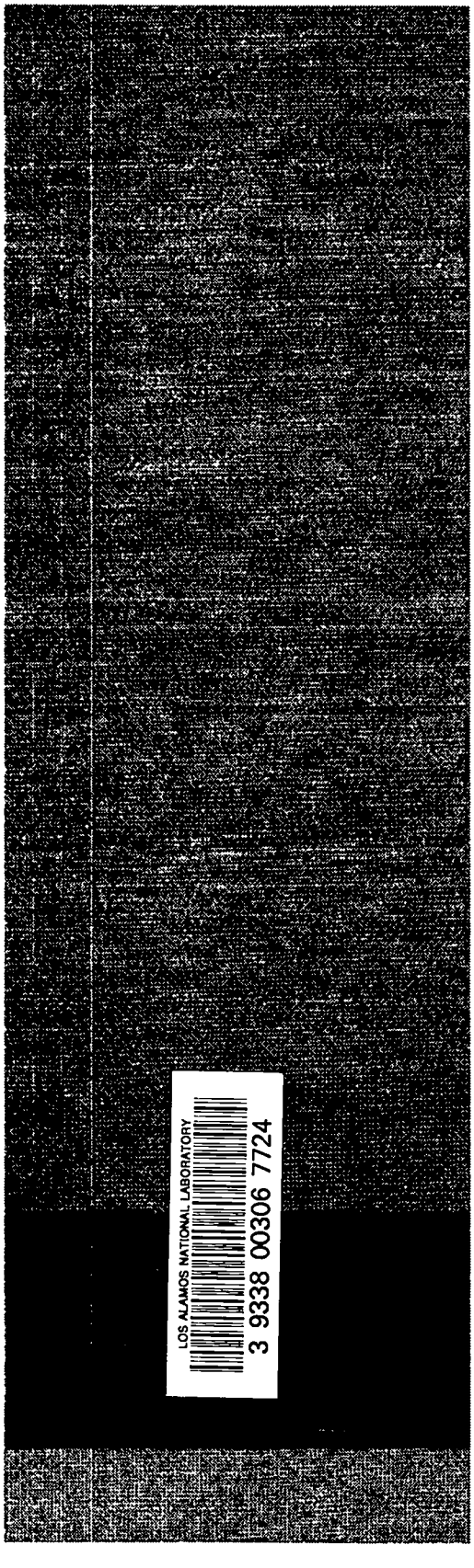

Calculation of a Shaped Charge Jet Using MESA-2D and MESA-3D Hydrodynamic Computer Codes

Los Alamos

Los Alamos National Laboratory is operated by the University of California for the United States Department of Energy under contract W-7405-ENG-36.

Edited by Patricia W. Mendius, Group IS-11

An Affirmative Action/Equal Opportunity Employer

LA-12274

UC-000
Issued: February 1992

Calculation of a Shaped Charge Jet Using MESA-2D and MESA-3D Hydrodynamic Computer Codes

John Bolstad
David Mandell

Los Alamos National Laboratory
Los Alamos, New Mexico 87545

CALCULATION OF A SHAPED CHARGE JET USING MESA-2D AND MESA 3-D HYDRODYNAMIC COMPUTER CODES

by

John Bolstad and David Mandell

ABSTRACT

The purpose of this project was three-fold.

1) **To study the effectiveness of the MESA 2D and the MESA 3D hydrodynamic computer codes for calculating the formation and penetration of a typical shaped charge jet.**

2) **To provide guidance to code users regarding mesh sizes and other code model sensitivities for calculating the formation and penetration of shaped charge jets.**

3) **To investigate the feasibility of a method for integrating both 2D and 3D code results for problems that are actually three-dimensional.**

This report summarizes some of the results obtained using the MESA 2D and 3D computer codes applied to a shaped charge jet formation and penetration problem for which there is experimental data. The accuracy of the code is investigated by comparing the code results with experimental data. Furthermore, the accuracy is assessed as a function of cell size in order to gain an insight into the approximations involved when performing a 3D calculation where mesh convergence is not practicable.

The feasibility of performing calculations such as these is explored by modeling the experiment using various approximations and determining how the accuracy is affected by these simplifications. Finally, the results of calculations performed with a 3D Cartesian geometry model are compared with calculations performed with a 2D cylindrical geometry model.

INTRODUCTION

Two- and three-dimensional numerical simulations of weapons systems and targets are a vital supplement to testing and perhaps even essential to use in the design/testing process. Typical applications and the uses for these codes in the design process for weapons or anti- weapons systems are described by Immele et. al.[1]. There are two basic types of codes for these applications, Eulerian and Lagrangian. There are many advantages and disadvantages to each type of code (these are summarized nicely by Anderson[2]). For problems with large material distortion, the users are generally led to analyze the event with Eulerian codes.

In the Eulerian description, the computation cells are fixed in space and the code calculates the flow of mass, momentum, and energy across the cell boundaries. Eulerian codes generally require much more computer time and resources to solve a problem to which they may be applied. Therefore with these codes, a greater emphasis is placed on numerical and modeling techniques that speed the computation. MESA is an Eulerian code, and this report concerns our experiences with it.

Most problems of interest require the use of a three-dimensional(3D) model, and 10^5 to 10^6 zones are usually used to model such a problem with an Eulerian code. Even this large number of zones sometimes represents a compromise between accuracy and cost (computer time). It does not appear possible to model and calculate a typical design problem with a zone size small enough such that mesh convergence is obtained with a 3D model.

Because of the cost constraints, it behooves the analyst to develop a strategy that will make use of the capability of a 2-D model in conjunction with a 3D model. The 2D model could, for example, be used to perform a cell size sensitivity study and examine details of features in the problem using a zoning so fine that mesh convergence is achieved. The 3D model is essential to gain an understanding of 3D features in the process being simulated and may be used to study, e.g., overall trends and 3-D geometry effects.

When such simulations are performed there are many questions that may remain unanswered. Typical questions that are often asked of the code developers by new code users when applying the code to a problem are the following.

1) How accurate is the answer? What cell size is required to obtain a given answer? How does the answer change with respect to the discretization cell size chosen for the simulation? How do the answers change when a variable grid is used rather than a uniform grid? How do the answers change when a moving mesh is imposed on the problem?

2) How do the computer code field length and computer charges vary with the number of cells in the problem?

3) How do results from two-dimensional and three-dimensional simulations compare?

4) How do the answers change when different material models are used to describe the materials in the simulation?

5) What physical dimensions/effects are so important that they must be modeled in order to achieve a meaningful answer? What dimensions/effects may be neglected or approximated without significantly compromising the answer?

6) What should be the role of two- and three-dimensional simulations in the design/analysis process?

These are just a sampling of questions that are asked by typical users. As the user's experience grows a feeling is acquired for how to best model a problem. Unfortunately, the answers to these questions can never by answered definitively by simulation of a single problem and more often than not, these questions are not answered in the code manuals or in papers describing the simulations that have been performed. This paper does not definitely answer these questions but will address many of them on a single typical application.

This paper describes our experience with modeling one particular experiment with the MESA-2D and MESA-3D computer codes. We have chosen to model a device that can be accurately modeled with the 2D code so that cell size and other parametric studies could be easily carried out. Experimental data exist for the device so that we may compare the calculations against actual data. We have also modeled the problem and simulated it with the 3D code in order to gain an understanding of the relationship between the results of the two codes and how they may be used together to solve a problem.

DESCRIPTION OF THE STANDARD CHARGE

We used as a basis for this calculation a shaped charge designed and used by the Ballistic Research Laboratory (BRL) in many of its experiments. This shaped charge was picked because it is described in unclassified reports and because some jet characteristics and penetration characteristics are reported for it in Refs. 3 and 4. This charge is shown in Fig. 1 and is described in Ref. 3. There appear to be many variations on this charge, some are described by DiPersio et. al.[4]. The particular charge that we used as a basis for our calculations, described in Ref. 3, used a 42° angle cone with a copper liner and it was charged with octal explosive and surrounded by an aluminum housing. The copper liner thickness is 0.20574 cm (0.081 in) and the cone outside diameter is 8.382 cm (3.3 in). The stated mass of the liner, explosive, and housing is 277, 875, and 517 grams.

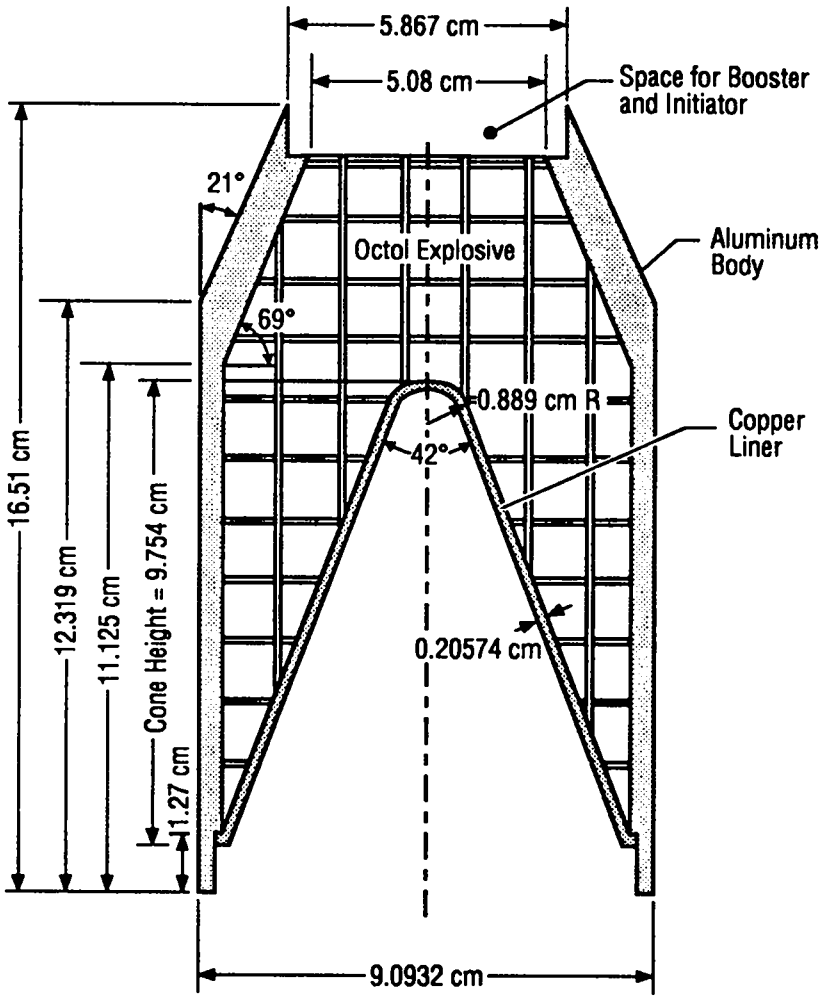

Fig. 1. The basic geometry and dimensions of the 3.3" dia. "precision" standard charge.

This particular charge is called the "precision" standard charge because its manufacture was carefully controlled so as to construct a charge with tolerances as small as possible on the wall thickness and concentricity of the liner. Experiments showed that the penetration of the precision charge was far superior to that of the non-precision charge. Experimental data are available for the jet tip velocity, the jet break-up time, and the location of the virtual origin. In addition, there is some penetration data available for the jet penetrating into 15.24 cm (6 in) diameter targets of Brinell hardness number 320 steel armor.

THE MESA CODE

MESA-3D is a three-dimensional, Cartesian, explicit, finite-difference Eulerian code with hydrodynamics, high explosives, and material strength models. A companion 2-D code, which has both Cartesian and cylindrical geometries, is available for scoping studies before detailed 3-D calculations, which take much more computer time, are run. The two- dimensional algorithms used have been described by Youngs[5]. The hydrodynamics is divided into two phases. The first phase is a pure Lagrangian calculation, and the second phase is a remapping back to the original Eulerian mesh. Since the advection (second phase) requires much more computer time than the first phase, the Lagrangian phase is sub-cycled. Typically we do four Lagrangian calculations for each remapping. Operator splitting is used. That is, the calculations are done in the x, y, and z-directions during one time cycle, and then in the z, y, and x-directions during the

next cycle. Van Leer[6] limiting is used in the advection phase in order to maintain steep gradients without introducing non-physical oscillations.

A unique feature of MESA is the interface reconstruction algorithm, which was developed by David Youngs[7]. This model allows fewer cells to be used for the same accuracy than were used in older codes since mixed-cell material interfaces are calculated accurately. The interface reconstruction method assures that materials are advected in the correct order.

Plasticity models include the Steinberg-Cochran-Guinan[8] model with work hardening and thermal softening, and the Steinberg-Lund[9] and Johnson-Cook[10] models with strain-rate hardening as well. The Mechanical Threshold Stress (MTS) model has also been implemented in MESA[11]. The von Mises yield criteria is used. Two fracture models have been implemented into the code. These include the Johnson (Jim) ductile spall model[12] and the Johnson (Gordon)-Cook fracture model[13].

We use the standard JWL[14] equation of state (EOS) for the high explosive (HE) and currently treat detonations with a programmed burn model in which the burn time for each cell is calculated a priori using the high explosive detonation velocity. A dynamic burn model is implemented in MESA but was not used in this study.

In addition to the JWL EOS for the HE detonation products, a number of analytical EOS equations are available for other materials. The Los Alamos tabular equations-of-state, SESAME[15], are also available in MESA.

Basic Two-Dimensional Model

Two types of the fixed Eulerian mesh are typically used with the MESA 2-D and 3-D codes; uniform or variable. The uniform mesh consists of a mesh description that uses cells that all have the same dimension in a given direction. The variable mesh contains cells whose dimensions in a given direction vary with position. The variable mesh is typically used in large problems because it allows a smaller mesh size in significant regions and a larger mesh size in regions that are relatively unimportant. The variable mesh technique is almost always needed for large 3-D problems because of the large number of mesh cells involved (a 3-D problem will typically require 10-100 times more cells than the number of cells required for a 2-D simulation).

For 2-D simulations, we may use either Cartesian or cylindrical geometry. Cartesian geometry is appropriate for problems that are plane strain, whereas cylindrical geometry is appropriate for problems that have an axis of symmetry. For the 2D simulations described here, cylindrical geometry was used. A large part of this study involves the sensitivity of the computed answers to the mesh size (this is typically called a cell size or noding study). Because the variable mesh description introduces another parameter into the test matrix, we have decided to use the simplest possible mesh description for our base case; i.e. the uniform mesh. For the base case calculation we used a mesh spacing of 0.05 cm in cylindrical *r-z* geometry. This represents a relatively coarse mesh size for the simulation considering that the copper liner thickness is only ~0.2 cm.

The computation grid for the base case is a uniform cylindrical geometry grid in both the *r* and *z* directions. The grid specifications for the base case are shown in Table I.

Table I

Computational Grid for the Base Case 2-D Calculation

Coordinate Direction	Number of Cells	Cell Size (cm)	Coordinate Limits (cm)
r	120	0.05	0 - 6.0
z	840	0.05	-17.0 - 25.0

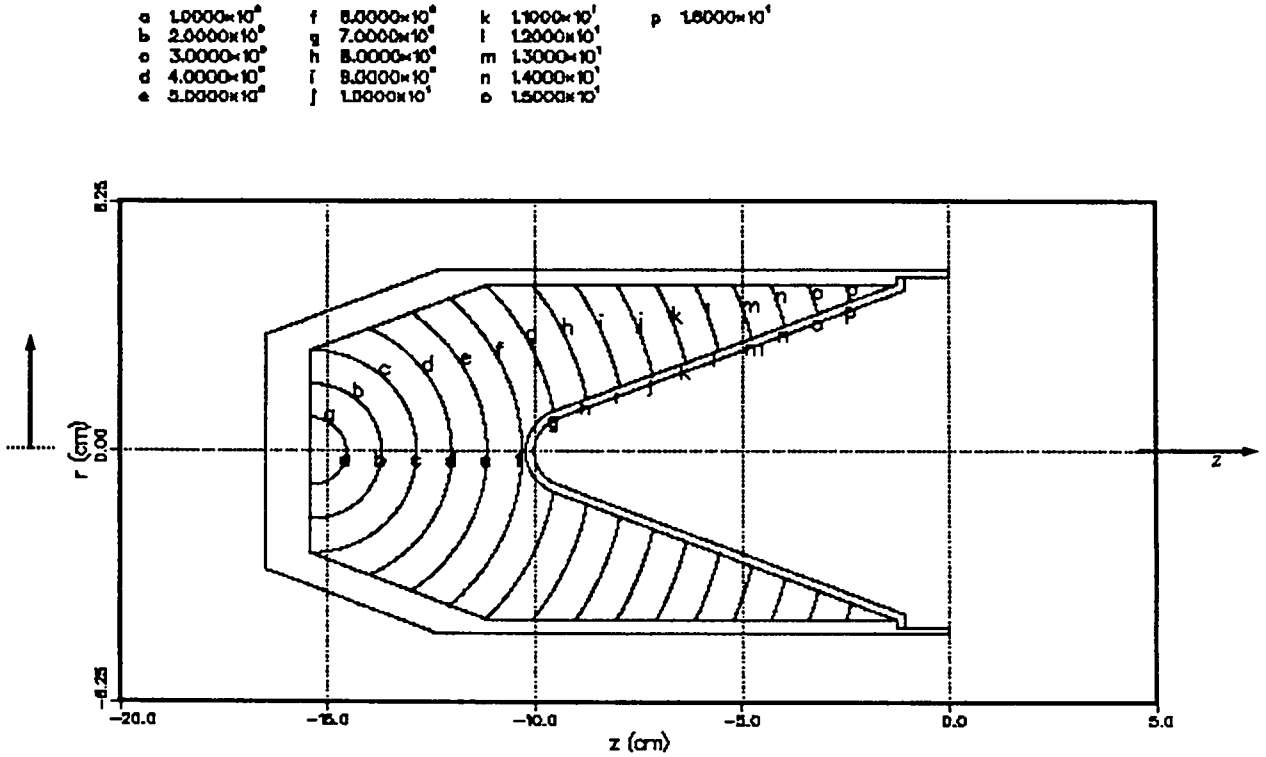

Fig. 2. Basic MESA-2D computer model for the shaped charge calculation showing the material interfaces for the MESA-2D computer model along with the calculated burn times for the Octol HE. All the HE is burned by ~17 μs.

This calculation contains 120 x 840 = 100,500 cells for a 2-D simulation. The computer model for this base case is shown on Fig. 2. The figure shows all the material interfaces between adjacent materials in a plane through the centerline of the model.

The calculation is initiated by igniting the programmed burn HE on the back surface centerline; this is at z = -15.4 cm and r = 0. The HE burn is simulated with the HE burn model in the code; this model calculates the HE detonation assuming a constant detonation velocity from the ignition point. For this calculation we used the standard detonation velocity of 0.848 cm/μs for the Octol provided by Mader[16]. The resulting burn times are shown in Fig. 2. The HE is burned in ~17 μs. The HE burn is simulated by inserting a given amount of internal energy, Δe, into the cell being burned. For the Octol HE in this device we used the standard value of Δe = 0.0527 Mbar-cm^3/gm found in the *matsdata* EOS data base.

The equation of state and strength models for the various parts of the device are listed in Table II. Additional details, along with the constants, are shown in Appendix I. The nominal yield strength for the copper is taken as Y_0 = 1.2 kbar. It is allowed to harden to 6.4 kbar in the Steinberg-Guinan model.

Table II

EOS and Strength Models for the Base Case 2D Model

Part	Material	EOS Type	Strength Model
Liner	Copper	Sesame Table Lookup	Steinberg-Guinan
Case	Aluminum	Gruneisen	none
HE	Octol	JWL	none
Background	Void	Void	none

The code calculates the masses of all the materials in the problem based on the dimensions and densities. The MESA-2D calculated mass of the three main components is compared to those reported by DiPersio et. al.[4] in Table III. The liner mass is matched quite closely but there are large discrepancies in the HE and case. The reason for the differences between the masses calculated from the dimensions and the actual reported mass is unknown.

Table III

Calculated vs. Reported Mass for the Standard Charge Components

Part	Calculated Mass (grams)	Reported Mass (grams)
Liner	279	277
Case	573	517
HE	912	875

Three-Dimensional Model

The MESA-3D code utilizes the Cartesian geometry; therefore the cell shapes are rectangular parallelepipeds. In order to save computer time and resources, many of the 3-D models utilize a mesh that is different in the axis and off-axis coordinate directions and also the cell sizes may vary along a single direction. In the 3-D code, the problem geometry and mesh specifications are specified in the FRAC-IN-THE-BOX input[17]. This input is shown in Appendix B for a uniform mesh size of 0.2 cm. This very coarse model utilizes 210 x 30 x 30 = 189,000 cells. For practical reasons (cost), finer mesh models require a variable mesh, and some of these have been utilized in this study; they will be discussed along with their results.

In order to provide a simple comparison between the 2-D and 3-D codes, the EOS and material models are kept the same. This is shown in a typical GENERATOR input deck for a 3-D simulation in Appendix B. The calculated mass for each component is the same in the 3D model as it was in the 2-D model shown in Table III. The HE detonation model and ignition point are the same as those for the 2-D model and code.

RESULTS OF JET FORMATION CALCULATIONS IN 2D AND 3D

The following sections describe in some detail the results of the numerical simulations with both the 2D and 3D MESA codes. We report on the effects of cell size, variable mesh, material strength models, contained vs. bare charge, forming the jet in air vs. void, sensitivity to a Galilean transformation on the mesh, sensitivity to the HE burn EOS parameters, and 2D vs. 3D simulations regarding the jet tip velocity. Finally we examine a simulation of the jet penetrating into a steel slab.

Jet Tip Velocity for MESA-2D Simulations

The key experimental data that we have to compare the calculation against is the jet tip velocity of ~8 cm/μs obtained by flash radiography. We first show how the jet tip velocity is determined from the computer simulations. Typical results for the base case 2-D simulation (0.5-mm mesh size) are shown in Fig. 3 where the interfaces between adjacent materials are shown at 20, 40, 60 and 70 μs. We are interested in obtaining the jet tip velocity as a function of time. This may be done by looking at the z-coordinate direction particle velocity along the $r = 0$ axis (i.e. for all z-values). The initial geometry and the coordinates for the computational grid are shown in Fig. 2. A profile plot of the particle velocity at $r = 0$ and t = 70 μs is shown in Fig. 4a. The velocity profile is almost linear with a peak (tip) velocity of 0.797 cm/μs. Finally, the tip velocity as a function of time is obtained by plotting the maximum velocity obtained from the profile plots for each dump time that was specified in the simulation. The axial profile maximum velocity is the tip velocity after ~40 μs. Before that time the maximum axial velocity in the jet is not at the tip but farther back in the jet. For example, the axial velocity profile at 20 μs is shown in Fig. 4b; at this time the maximum velocity is ~1.3 cm behind the tip.

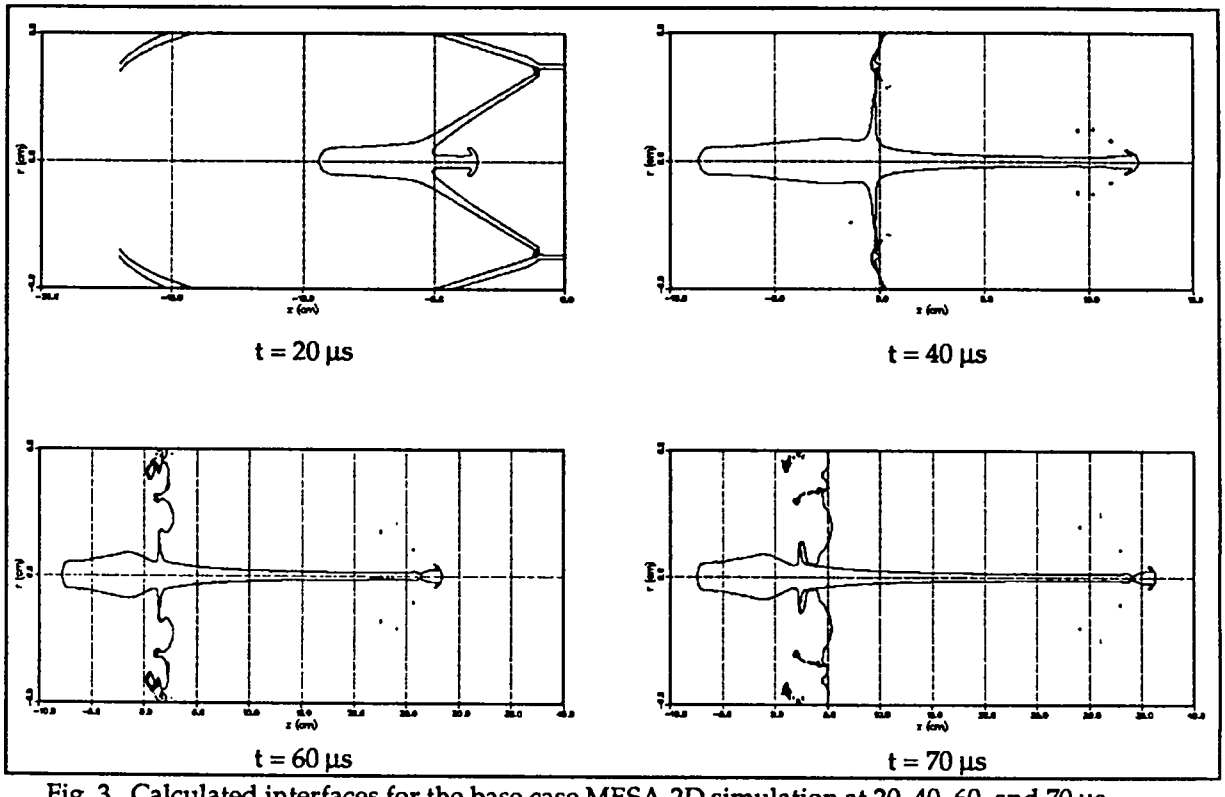

Fig. 3. Calculated interfaces for the base case MESA-2D simulation at 20, 40, 60, and 70 μs.

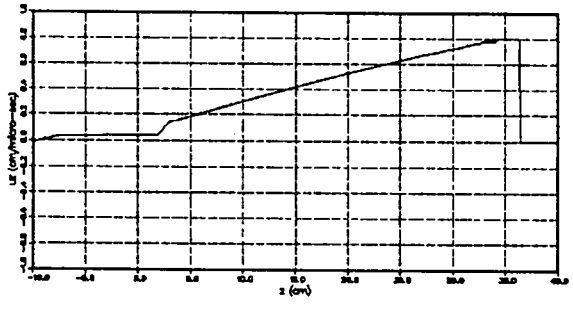

Fig. 4a. Profile plot of the centerline z-velocity component at 70 μs. The tip velocity is 0.797 cm/μs.

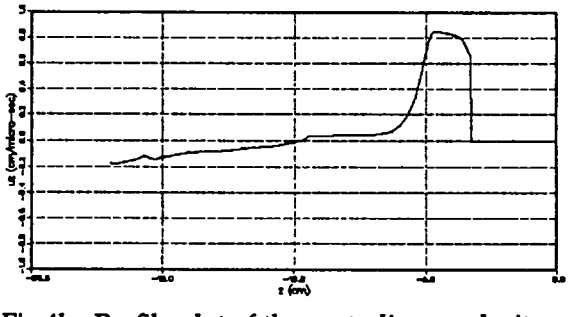

Fig 4b. Profile plot of the centerline z-velocity component at 20 μs. The maximum velocity is 0.85 cm/μs. The tip velocity is less (~0.68 cm/μs).

Additional calculations were performed for uniform mesh sizes of 1/4, 1, and 2 mm. The results for the maximum axial velocity as a function of time for the different mesh sizes are shown in Fig. 5. There are a number of interesting features of the calculation that can be observed from the figure. 1) The maximum axial jet velocity does not necessarily tend to an asymptotic limit with increasing time (or distance). 2) The calculation with the 1/4 mm cell size converges to a value of 0.814 cm/μs by 45μs; the simulations with larger cell sizes do not converge to a steady-state value during the simulation time. 3) As the cell size increases, the predicted jet tip velocity tends to a smaller value. It appears as though the calculated tip velocity might converge to the experimental measurement of 0.83 cm/μs. 4) For the larger mesh size simulations, the jet tip velocity continues to drop off with time rather than converging to a limit value. 5)

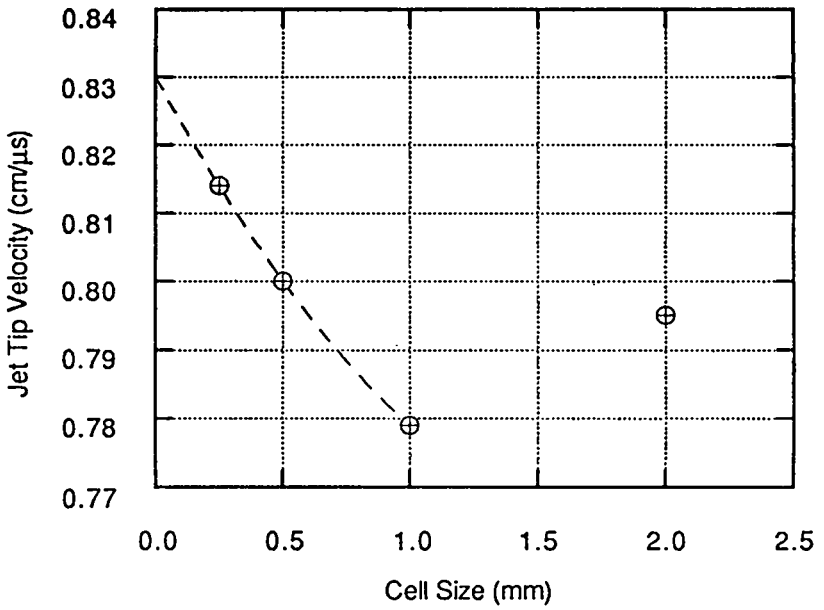

Fig. 5. The MESA-2D predicted maximum axial velocity as a function of time for calculations using mesh sizes of 1/4, 1/2, 1, and 2 mm. The measured jet tip velocity is 0.83 cm/μs.

Quite small mesh sizes (~1/4 mm for this device) must be used in the simulation in order to obtain convergence to the correct tip velocity. The fact that the jet tip velocity drops off with distance is in accordance with experiments and the findings of DiPersio (Ref. 3, pg. 179, Ref. 4, pg. 26): *"the decrease in jet particle velocity its proportional to the distance traveled through the air and is independent of its initial velocity"*. DiPersio suggests that the jet-tip velocity decrease may be due to air drag, but these results suggest that there may be other hydrodynamic factors since air drag is not included in this calculation and we see the equivalent result.

The jet tip velocities at 50 μs, obtained from Fig. 5, are plotted as a function of cell size in Fig. 6. This figure demonstrates that the jet tip velocity tends to converge to the experimental value as the cell size is decreased. Unfortunately, it also shows that within the range of cell sizes investigated here, the tip velocity does not converge and it appears as though the experimental value will be predicted only when the cell size tends to zero. Especially interesting is the result obtained for a 2-mm cell size. The reason for this apparently good prediction using this relatively coarse mesh size is not understood. One possible cause for this anomalous behavior may be that the cell size is too large compared to the other important dimensions in the problem. Remember that the liner thickness is ~2-mm and thus the cell size is basically the same as the liner thickness. We know that in order to produce good results in these kinds of hydrodynamic simulations, we need a number of cells through the thickness of the structure. Furthermore, this is the only simulation conducted where the jet radius is smaller than the cell size. It may be that there is some difference in the material transport algorithm under this circumstance. Based on these considerations, it could be that the apparently good prediction with the 2-mm cell size is just fortuitous. Because of this anomalous behavior, we decided to perform a complete cell size study of this problem using the MESA-2D code and the 2D model described above.

Cell Size Study for the Mesa-2D Simulations

A cell size study of the 2D model and code was conducted because of the unexplained behavior of the result obtained from the 2 mm cell size simulation shown in Fig. 6. Additional simulations were performed at cell sizes of 0.75, 1.25, 1.50, 1.625, 1.875, and 2.5 mm. These sizes were chosen to confirm or eliminate the possibility that the 2-mm cell size point in Fig. 6 was due to an input specification error during the 2D simulation. The jet tip velocities at 50 μs for all cell sizes are shown in Fig. 7.

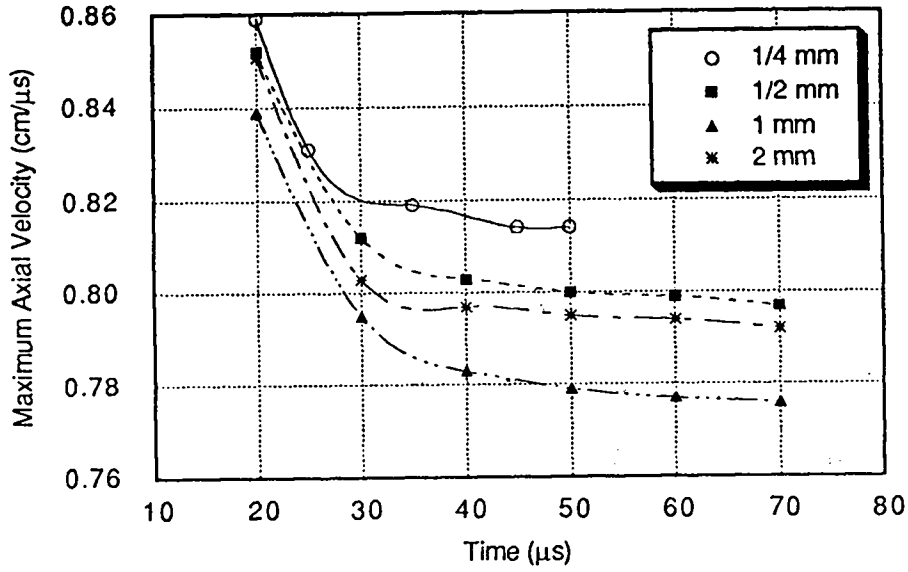

Fig. 6. The calculated jet tip velocity at 50 μs as a function of cell size.

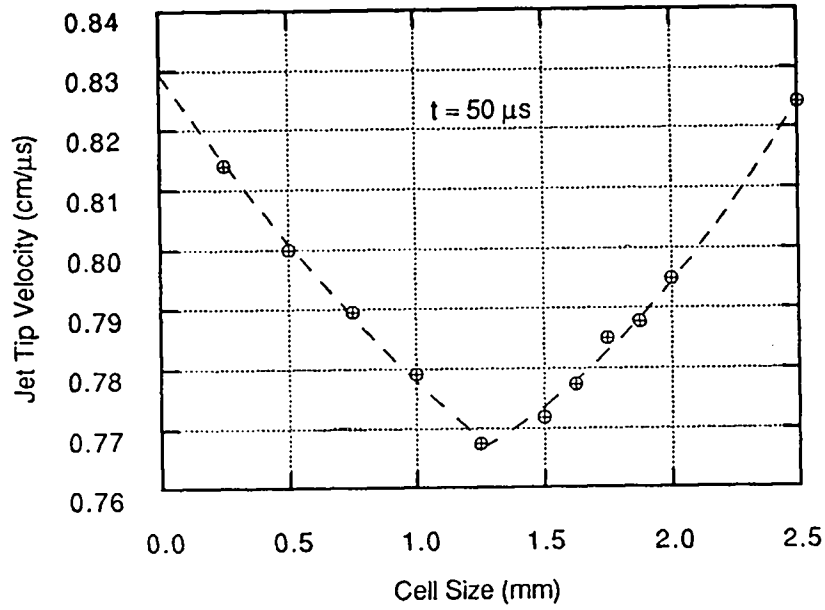

Fig. 7. Cell size study focusing on the calculated jet tip velocity at 50 μs.

The figure shows a break point at ~1.25-mm cell size. The data points in this figure are fit using a quadratic in each of the two different regions. It is obvious that something significant changes in the model at ~1.25-mm. The behavior of this curve is not well understood but it does illustrate the hazards involved in making predictions from a single simulation especially when the focus is on a single parameter not directly predicted by the partial differential equations contained in the code model. It is quite interesting to note that as far as the jet tip velocity is concerned, the crudest model (2.5 mm) gives a better prediction than the

best model. Looking closer at the details of the calculation would probably show that the simulations with a cell size greater than 1.25 mm have diminished validity.

One clue about the behavior of the larger cell size simulations is demonstrated in Fig. 8. This figure shows the liner interfaces overlaid on a cross section of the computational mesh for the 1.25 mm mesh size model. The figure shows that, at this mesh size, there are only a few pure cells in the liner. At cell sizes larger than this, there will be very few if any pure cells in the liner; they will be essentially all mixed cells. It would not be expected that the code could simulate the plastic strain and material flow processes when it has such a coarse mesh description.

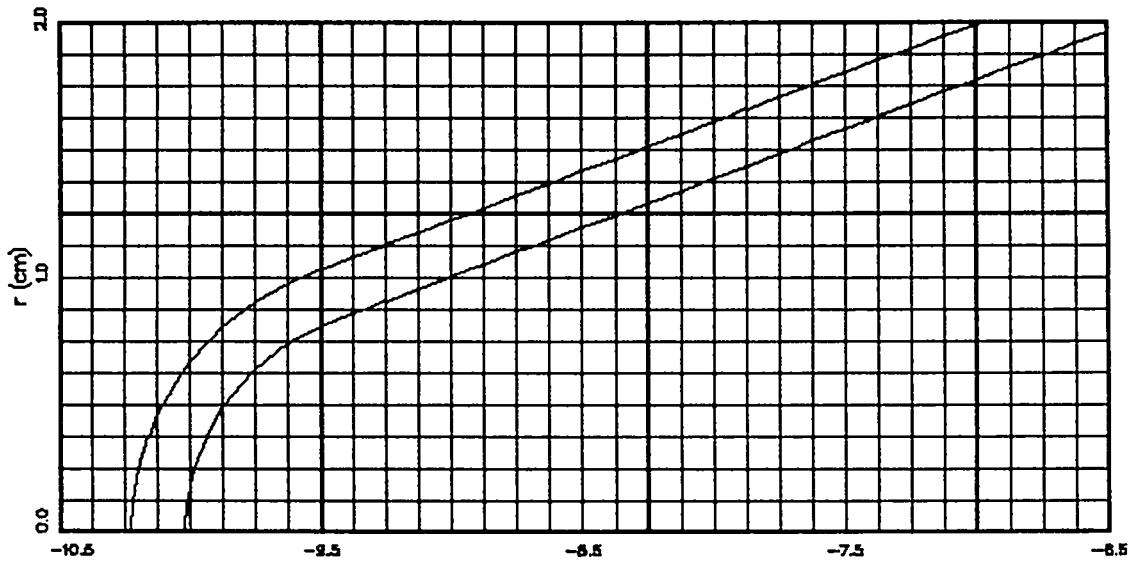

Fig. 8. A close up view of the computations cells with the liner interfaces superimposed on the computational grid for the simulation with uniform 1.25-mm cell sizes.

Effect of Variable Mesh Spacing

For many problems, it is not feasible or prudent to use a uniform grid in the computer model. In 3D simulations, for example, it is almost never practical to use a uniform grid with a sufficiently small cell size. Even in 2D simulations, it is often desirable to use a variable grid to decrease the number of cells in a problem. The main goal when specifying a variable grid is to use sufficiently small size cells where they are needed (e.g. at an interaction zone) and allow the cell sizes to grow in regions where their large size is not an important contributor to the desired answer. It is generally thought that large aspect ratio cells decrease the accuracy of the calculation. Generally, experience and judgement are used to specify a variable grid, and the effect of the grid design on the answer is not known.

In order to examine how a typical variable grid design would affect the accuracy of the Standard Charge simulation, we have performed a 2D simulation using a variable grid design that a typical user might employ. The base case uniform 0.5 mm grid is used as a basis for the variable grid. In this scheme, we have kept the cell width in the axial direction at a uniform 0.5-mm and used a uniform expansion of the cell widths in the radial direction. In the radial direction we started with a 0.5-mm cell size at the origin and increased each succeeding cell thickness by a factor of 1.05. This scheme ended up using only 40 cells in the radial direction (from r=0 to r=6 cm) compared with 120 cells for the base case simulation shown in Table I. This means that this model uses only 1/3 the number of cells as does the base case and will need only ~1/3 the computer resources. The cell shapes for part of the problem are shown in Fig. 9. The cells near the origin have a size and shape nearly the same as for the uniform grid case, whereas those near the

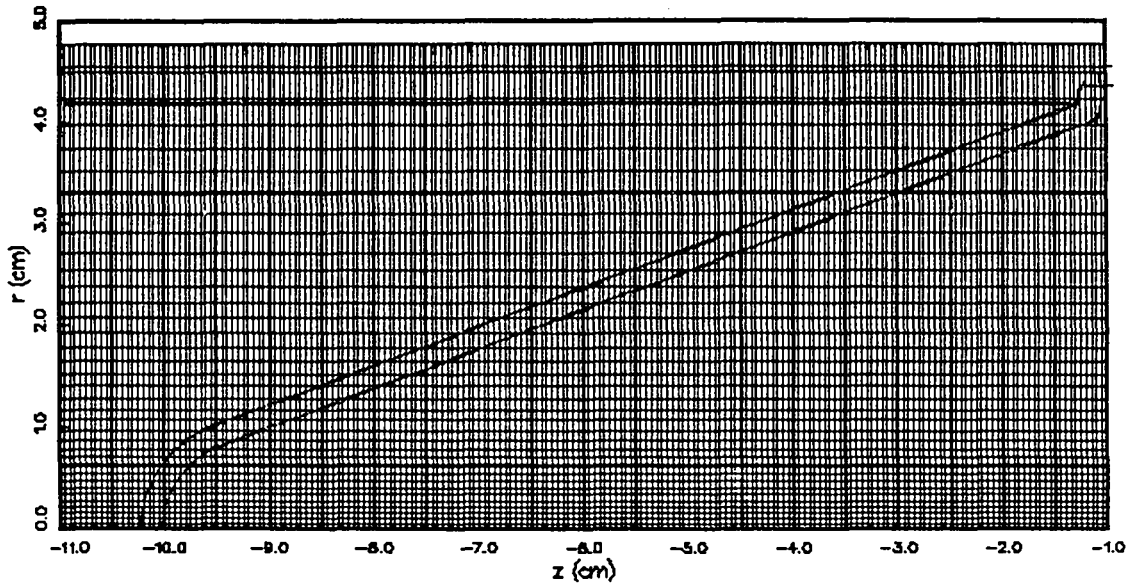

Fig. 9. A close up view of the computations cells with the liner interfaces superimposed on the computational grid for the simulation with a variable grid spacing in the radial direction and a uniform grid spacing in the axial direction.

outer radius of the problem have a large aspect ratio. The worst cell at r=6 cm has a Δr of 3.3-mm and an aspect ratio of $\frac{3.3}{0.5} = 6.6$.

This model was run with the MESA-2D code keeping all other parameters the same as the base case. The simulation with the variable mesh produced a calculated jet tip velocity of 0.793 cm/μs at 50 μs. This is within 1% of V = 0.800 cm/μs at 50 μs obtained from the base case calculation. For this experiment, we are able to obtain essentially equivalent results for the tip velocity using only 1/3 the computer resources. For this simulation, use of the variable mesh was a very productive tool, and its effect on the predicted jet velocity was negligible.

Sensitivity to Relative Velocity

For many problems of interest, it is desirable to keep a certain portion of the simulated space relatively stationary with respect to the Eulerian grid. This approach may be taken, e.g., to decrease the amount of advection between cells and therefore increase accuracy in the region of interest. Another reason for this approach is to decrease the number of cells required to model the problem by keeping a moving object relatively stationary in the grid. This is accomplished in MESA-2D and MESA-3D by imposing a Galilean transformation of the problem. This is accomplished in MESA by modifying all velocity components in a given direction according to the rule $v' = v - u$, where v is the original velocity component, v' is the transformed velocity component, and u is the Galilean transformation velocity. The Galilean transformation may be performed in one or more directions.

It is known that the Galilean transformation will affect the problem results but it is difficult to quantify the exact effect. It is generally thought that the accuracy of the simulation will be increased in the region where the material velocities are made smaller with respect to the grid and less accuracy in regions where the material velocities are increased.

In order to investigate the effect of a Galilean transformation on this problem, we have modified the base case to simulate it with a Galilean transformation where the jet tip is held relatively stationary in the Eulerian grid. This was accomplished by restarting the base case simulation at 20 μs and at that time introduc-

ing a Galilean transformation of 0.8 cm/μs into the grid. Since the tip velocity is known to be ~0.8 cm/μs, this has the effect of keeping the jet tip stationary in the grid at later times. The predicted jet tip velocity in the transformed system is compared with that of the base case at 50 μs.

The base case tip velocity was 0.800 cm/μs at 50 μs, and the simulation with the mesh moving at 0.8 cm μs predicts a tip velocity of 0.805 cm/μs at 50 μs. The results compare almost exactly (< 1% difference) with the moving grid simulation giving slightly better agreement with experiment.

Effect of Material Strength Models

Early theories of jet formation from conical shaped charges made the simplifying assumption that strength effects in the liner could be ignored because the pressures at the stagnation point are much higher than the material strength of the liner (Ref. 3, pg. 72). In the same reference (pg. 96), a simple hand calculation is performed that shows that pressures of the order of 0.7 Mbar could be expected at the stagnation point for a shaped charge with a copper liner. Examination of our base case calculation shows that pressures exist near that value (~0.78 Mbar) at 20 μs. Arguments such as these lead to the conclusion that the liner material strength may be neglected in the calculation, i.e. the calculation may be performed using the hydrodynamic assumption whereby the materials are treated as fluids.

We performed three calculations to investigate the sensitivity of the predicted jet velocity to the type of yield (strength) model for the liner used in the calculation. 1) We used the Steinberg-Cochran-Guinan (S-C-G) model[8] with the default constants for OFHC copper given in Ref. 8. This model is our base case calculation previously described; the strength constants are shown in Appendix A, MESA-2D Generator input. 2) We used the base case model except we changed the plasticity model for the liner from the Steinberg-Guinan to the Johnson-Cook strength model[10]. We used the constants for OFHC copper given in Ref. 10. 3) We performed a simulation using the hydrodynamic assumption, no material strength. A summary of the yield strengths used in these models along with the calculated jet tip velocity at 50 μs is summarized in Table IV. Since strain hardening and thermal softening are included in the models, two values of the yield strength are given: the nominal value and the maximum allowed value.

Table IV

Strength Models, Yield Strengths, Calculated and Experimental Results

Strength Model	Initial Yield Strength	Max. Yield Strength	Jet Tip Velocity
S-C-G	1.2 kbar	6.4 kbar	0.800 cm/μs @ 50 μs
Johnson-Cook	0.9 kbar	6.4 kbar	0.813 cm/μs @ 50 μs
Hydrodynamic	0	0	0.864 cm/μs @ 50 μs
Experiment			0.830 cm/μs

The results of this study show that the jet tip velocity is over-predicted if strength is neglected. We see that the S-C-G model, the model with the highest initial yield strength predicts the lowest jet velocity whereas the Johnson-Cook model predicts an intermediate result. The conclusion reached from this small parametric study is that it is necessary to include material strength in the calculation as it is an important contributor to the calculated jet velocity. The trends indicate that higher strengths in the model produce lower predicted jet velocities.

Effect of Contained vs. Bare Charge

We now turn to the sensitivity of the answer to various modeling approximations that could reasonably be made to simplify the actual experiment. The first is the effect of the case on the jet tip velocity. If we can model just the bare charge and neglect the case, the setup time will be shorter, and the computation will be simplified because there is one less material in the problem. In addition the computation should be speed-

ed up since there will be fewer mixed cells in the simulation. The question is, how much is the tip velocity affected if we neglect the case?

In order to examine the effect of containment on this shaped charge configuration, we reran the base case (i.e. 1/2-mm cell size) with the casing eliminated from the simulation. For this simulation, the predicted jet velocity is lower as would be expected. The predicted jet tip velocity at 50 μs is 0.788 cm/μs compared with 0.800 cm/μs for the base case (i.e. with confinement). This is a difference of 1.5%. For many applications such as scoping studies, this error would be acceptable considering the savings in modeling and computer time. This run used ~10% less CPU charges than the base case simulation.

Effect of Forming Jet in Air Instead of Void

The motivation for forming the jet into a void rather than an air background is similar to that of neglecting the case. The EOS for a void material is much simpler than that for air, and this leads to a computational simplification in the many mixed cells containing the background material. By simulating the background material with void rather than air, the computation should be faster. However it is speculated that air drag on the jet particles offers a significant retarding force on the jet and could significantly affect its predicted velocity in the simulation.

In order to examine the effect of forming the jet in an air background rather than a void, we reran the base case with air as the background material. For this simulation, the predicted jet tip velocity at 50 μs is 0.798 cm/μs compared with 0.800 cm/μs for the base case. This is a difference of only 0.25% and indicates that it is not necessary to form the jet into an air media. The running time for the two computations was similar so that there is very little incentive to replace air with void in these types of calculations.

Sensitivity to HE Burn EOS Parameters

The JWL equation of state[14] for high explosive detonation products is used in the MESA codes along with the programmed burn model. The pressure, P, for detonated HE products is calculated from the relative specific volume of the products ($V = \rho_0/\rho$) and their specific internal energy per unit initial volume E [Mbar].

$$P = A\left(1 - \frac{\omega}{R_1 V}\right) e^{-R_1 V} + B\left(1 - \frac{\omega}{R_2 V}\right) e^{-R_2 V} + \frac{\omega E}{V}$$, where

R1, R2, and ω are dimensionless constants, and A and B are adjustable constants with units of pressure. The initial energy of the detonation products, e_0 [Mbar-cm^3/gm] is also specified.

The basic programmed burn model assumes that the detonation wave travels in all directions at a constant velocity equal to the Chapman-Jouguet (CJ) detonation velocity, D. The times at which the wave arrives and leaves a particular cell are calculated, and the HE energy is deposited linearly in that cell during the time interval that the detonation wave is within the cell[18].

Since the constants for the JWL EOS are usually obtained from cylinder tests[19] and may not be correct for other simulations, we performed a parametric study to determine the sensitivity of the tip speed to variations in the input constants. In order to determine the effect of the JWL constants on the standard charge tip speed we varied several of the constants and repeated the base mesh calculation. The JWL constants must be changed in a consistent manner. This involves the solution of three simultaneous equations[20].

The CJ pressure, P_{CJ}, is a sensitive parameter in the prediction of HE waves. The reported experimental P_{CJ} for octal is 0.343 Mbar[16]. We varied this value ±10 Kbar. Near the CJ point the high pressure behavior is dominated by the coefficient R_1 in the first exponential term of the JWL equation (Ref. 14). We varied R_1 +10 percent and - 5 percent (The - 10 percent case resulted in B_2 being negative. and we decided not to use this case). The largest expansion obtained in the cylinder tests is a sevenfold increase in the volume of the detonation products and the corresponding energy is E_7. This energy is taken as a measure of the available energy for driving the cylinder walls[20]. We varied this energy ±10 percent in order to determine its effect

on the jet tip speed. A consistent set of constants was obtained in each case by varying e_0, A, B and R_1 ρ_0; D, ρ_0, and R_2 ρ_0 were held constant. The constants used are shown in Table V. Physically all of the JWL constants should be positive, but in three cases 1b (P_{CJ} = 0.353 Mbar), 1d (R_1 = 1.1 x base), and 1f (E_7 = 0.9 x base), the constant C in the JWL equation for the isentrope[14], P_s

$$P_s = Ae^{-R_1\rho_0 V} + Be^{-R_2\rho_0 V} + CV^{-(1+\omega)}$$

was slightly negative. The isentrope was positive over the range of interest.

Table V

Input and Other Constants

Input Constants#	Simulation						
	Base Case P_{CJ} = 0.343 Mbar	P_{CJ} = 0.333 Mbar	P_{CJ} = 0.353 Mbar	R_1 = 1.10 x base	R_1 = 0.95 x base	E_7 = 0.90 x base	E_7 = 1.10 x base
e_0[Mbar-cm^3]	0.0527	0.06161	0.0440	0.03575	0.06216	0.039302	0.066215
A	7.486	7.747	7.240	9.441	6.698	7.5967	7.3747
B	0.1338	0.06359	0.20246	0.2874	0.0460	0.17218	0.095189
R_1	4.50	4.50	4.50	4.95	4.27	4.50	4.50
Calculated Values							
P_{CJ} (Mbar)	0.343	0.333	0.353	0.343	0.343	0.343	0.343

In addition we used the constants D = 0.848, ρ_0 = 1.821, R_2 = 1.2, and ω = 0.38 for all runs.

The jet tip velocity results are shown in Table VI for the base case and for the JWL constant variations discussed above. Since the base case calculation resulted in a jet tip velocity that was a little low, the calculation with a CJ pressure lower than the reported 0.343 Mbar would be expected to be too low also, and this trend is seen in Table VI. The tip velocity for a P_{CJ} of 0.353 Mbar is 0.817 cm/μs which is higher than the base case 0.800 cm/μs but still below the measured 0.83 cm/μs. The maximum observed pressures are well below P_{CJ}, which is a well known characteristic with programmed burn and coarse meshes and is thought to be due to the large cell sizes relative to the detonation reaction zone and the time step size[21]. The velocity is 0.827 cm/μs for the higher R_1 calculation and 0.785 for the lower R_1 case. The case with R_1 1.1 times the base case value results in a jet tip speed very close to the measured value, but the maximum calculated pressure still does not reach a value near P_{CJ}. A 10 percent change in R_1 results in a 3.4 percent change in the jet tip speed. The E_7 variation resulted in only small changes in the jet tip speed.

Changes in the JWL constants result in small changes in the shaped charge final jet tip speed and it appears that the uncertainty in the JWL constants is not a serious problem in this case. It also appears as though it is not a requirement for the calculated pressure to be the *CJ* pressure in order to obtain a good simulation.

Table VI

Results of JWL Sensitivity Study

Run Description	2D Jet Tip Velocity at 50 μs (cm/μs)	Detonation Pressure at 10 μs (Mbar)
Base Case P_{CJ} = 0.343 Mbar	0.800	0.286
P_{CJ} = 0.333 Mbar	0.782	0.272
P_{CJ} = 0.353 Mbar	0.817	0.292
R_1 = 1.1 x base	0.827	0.287
R_1 = 0.95 x base	0.785	0.285
E_7 = 0.9 x base	0.798	0.284
E_7 = 1.1 x base	0.803	0.284

Comparison of 2D and 3D Calculation

One of the goals of this study was to relate 2D calculations to 3D calculations to determine the consistency in predictions between the two codes. There are two reasons for this part of the study. First, since 3D calculations are much more costly in computer time than 2D calculations, we typically would like the majority of design studies to be 2D and then run only a small number of 3D runs in order to study the 3D effects. Second, it is not generally practical to run a sufficiently fine mesh in 3D to achieve mesh convergence. In order for this method (combing the results of 2D and 3D calculations) to work, there must be agreement between the codes. The models are the same in the two codes, but there are some differences in defaults and coding. In order to check on this, three problems were run with both the 2D and 3D codes; in principal the results should be the same since it is really a 2D (axially symmetric) problem that is being simulated.

It did not seem productive to run 3D simulations of the existing 2D models because the number of mesh cells required for a meaningful run would be prohibitive. We decided to run simulations with the 3D code that are typical of those usually employed by the analyst.

A variable mesh spacing is usually employed in 3D calculations. Typically, we allow the cell sizes to vary with a ratio between adjacent cells of 1.1 or less, depending on the maximum number of cells we are willing to use. We used a constant mesh size in the majority of this study to eliminate the uncertainty of this process from our consideration. Three problems were devised to compare 2D and 3D results. They were designed so that they could be easily calculated with the 3D code but still use a small enough cell size to be meaningful. The models consist of a uniform 1-mm cell size in the axial (z) direction and a variable cell size in the radial (x,y in 3D or r in 2D) direction. The variable mesh in the radial direction started with a 1-mm radial cell size at the origin and then expanded this size by a ratio of ~1.05 or 1.1 for adjacent cells. Two of the simulations were performed in the hydro (no strength) mode and one was run with the Steinberg-Cochran-Guinan strength model in the liner. The detailed input for the model with strength and a 1.1 expansion ratio is shown in Appendix B.

The calculated results for the three simulations are shown in Table VII. For the hydro run with a 1.05 expansion factor, the calculated jet tip velocity at 50 μs was the same from both the 2D and 3D codes. The results agree to within 0.4% for both the runs with the 1.1 mesh expansion factor. This good agreement indicates that for the same geometrical setup, the 2D and 3D codes give comparable results. Furthermore, comparing the last run with a 2D simulation with uniform 1-mm cell sizes shows that the variable mesh simulation gives good accuracy (~1%) while significantly reducing computer costs by a factor of ~2.5.

Table VII

Comparison of 2D and 3D Calculations

Mesh Description	Strength or Hydro Calculation	2D Jet Tip Velocity at 50 μs (cm/μs)	3D Jet Tip Velocity at 50 μs (cm/μs)
1.05 expansion in x & y 1 mm constant in z-direction	hydro	0.822	0.822
1.1 expansion in x & y 1 mm constant in z-direction	hydro	0.810	0.807
1.1 expansion in x & y 1 mm constant in z-direction	strength	0.774	0.771

Table VIII

CPU and Field Length for Selected Simulations

Type of Run (2D or 3D)	Cell Size (mm)	*r* by *z* (2D) *x* x *y* x *z* (3D) No. of Cells	Total Number of Cells	CRAY Field Length (MWords)	CPU at 40 μs (min)
2D	2	30 x 485	14,550	1	2
3D	2	30 x 30 x 210	189,000	10	91
2D	1	60 x 770	46,200	2	7
2D	1/2	120 x 840	100,800	4	35
2D	1/4	240 x 1480	355,200	13	207
3D (hydro)	variable *y* & *z* 1*x*	20 x 20 x 420	168,000	7	153
3D	variable *y* & *z* 1*x*	20 x 20 x 420	168,000	12	177
2D	variable *r* - 1 *z*	20 x 570	11,400	1	3

Summary of Run Parameters – Field Length and CPU Time Required

The CPU time (at 40 μs simulation time) and CRAY Field Length are shown in Table VIII for a number of selected simulations. All of these simulations include strength in the computer model except for the one 3D run labeled "hydro". The field length is important because it determines the computer resources needed to run the simulation. At the time of this study, e.g., 16 Mwords was the limit for MESA simulations at Los Alamos (this restriction has since been relaxed). The table shows the large increase in both field length and CPU required as the cell size is decreased. For example, a uniform 1/4-mm cell size was about the smallest that could be easily simulated with MESA-2D, and it takes ~100 times more CPU to simulate the problem with 1/4-mm cells than with 2-mm cells. While the field length is roughly proportional to the number of cells, the CPU increases by a factor of 4-7 when the cell size is decreased by a factor of two.

The comparison between 2D and 3D calculations shows that the 3D code takes ~45-60 times the CPU as does the 2D code (but there are 13-15 times as many cells in the 3D model). This shows the efficacy of doing as much of the simulation as possible in 2D. Finally, the two 3D runs that are identical except for the strength models shows that the field length increases by ~70% in the 3D code when strength is modeled but the CPU only increased by ~16%. Since strength is so important in the simulation, it does not appear that the small savings in CPU offsets the loss of accuracy in the calculation.

JET PENETRATION INTO STEEL

The following sections describe a calculation performed to predict the penetration of the jet (from the "standard charge") into a steel billet. There is some penetration data available, and we will compare the predicted penetration with that measured at a standoff of 2 charge diameters(CD). The experiments showed that the penetration of the jet varied by a large amount, especially at large standoffs[4]. It was found that jets from charges made with a higher degree of precision penetrated much deeper than those made to a lower precision standard. Examination of radiographs showed that this was due to jet waver (departure from straight-line travel). Since the MESA models assume that the jet is perfectly aligned, the computer simulations predict penetration from an "ideal" jet, i.e., one manufactured with perfect precision (symmetry), we expect that the MESA simulations will overpredict penetration.

The Experiment

The copper jet from the "standard charge" was fired into a 15.24-cm dia. steel billet of Brinell hardness number 320 (BHN 320) in order to obtain penetration data[4]. The experiment was repeated many times at standoffs of 2, 5, 8, 12, and 25 CD. Two different types of charges were made with respect to the manufacturing tolerances of the case and liner dimensions. A charge manufactured with tolerances as tight as possible is called a "precision charge," and one with rather loose tolerances is called a "non-precision charge". Because of the repeated experiments, an idea of the variability of the penetration was obtained. The results of the experiments are shown in Fig. 10. The figure shows that there is a higher degree of reproducibility in the experiments at the lower standoffs with much more scatter in the data at high standoffs. It also shows that the performance of the "non-precision" charges are degraded with respect to that for the "precision" charges. We decided to simulate the experiment at 2 CD standoff partially because of the repeatability of the experiment at this standoff and partly because the simulation becomes much more costly at the larger standoffs.

The Mesa-2D Model For The Penetration Calculation

Jet penetration was calculated by inserting a steel target into the calculational grid at a location two charge diameters from the base of the liner. This was accomplished by using the MESA WINDOW operation on the dump taken at 40 μs during the base case jet formation calculation (0.5 mm cell size). A Galilean transformation was performed on the system so that the reference frame was moving at 0.25 cm/μs in the z-direction. This has the effect of having the billet move at 0.25 cm/μs to the left in Fig. 11. The calculation was resumed at this time and the jet first strikes the target at ~44 μs. The initial geometry for this calculation is shown on Fig. 11.

We used a SESAME EOS (number 4270) for the target material and an elastic-plastic strength model. We used a yield strength of 11.1 kbar for the steel target material.

Results of the Jet Penetration Calculation

We simulated the experiment for 320 μs; this is ~ 276 μs after the initial jet impact. Typical results from the simulation are shown in Fig. 12 where the interfaces between materials are shown for times of 60, 140, 220, and 320 μs. The billet is moving to the left at 0.25 cm/μs in the coordinate system shown in Fig. 12. The predicted penetration for the simulation was obtained from results such as those shown in Fig. 12 and plotted as a function of time; these results are shown in Fig. 13.

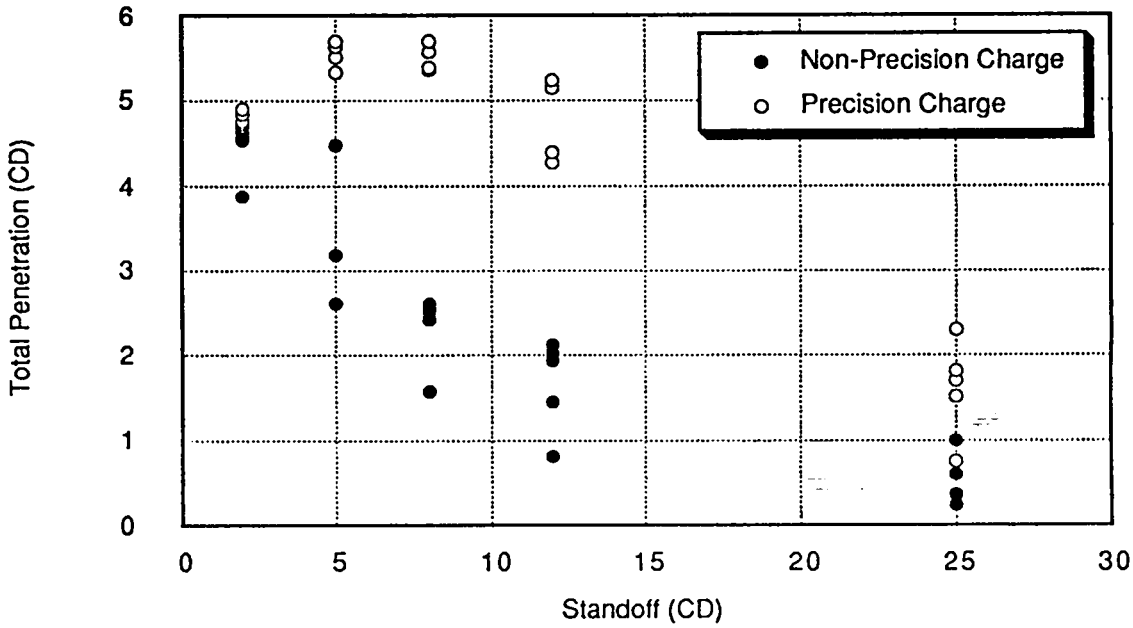

Fig. 10. Total penetration as a function of standoff between the base of the charge and the front of the target for "precision" and "non-precision" charges. The scatter in the data increases with standoff.

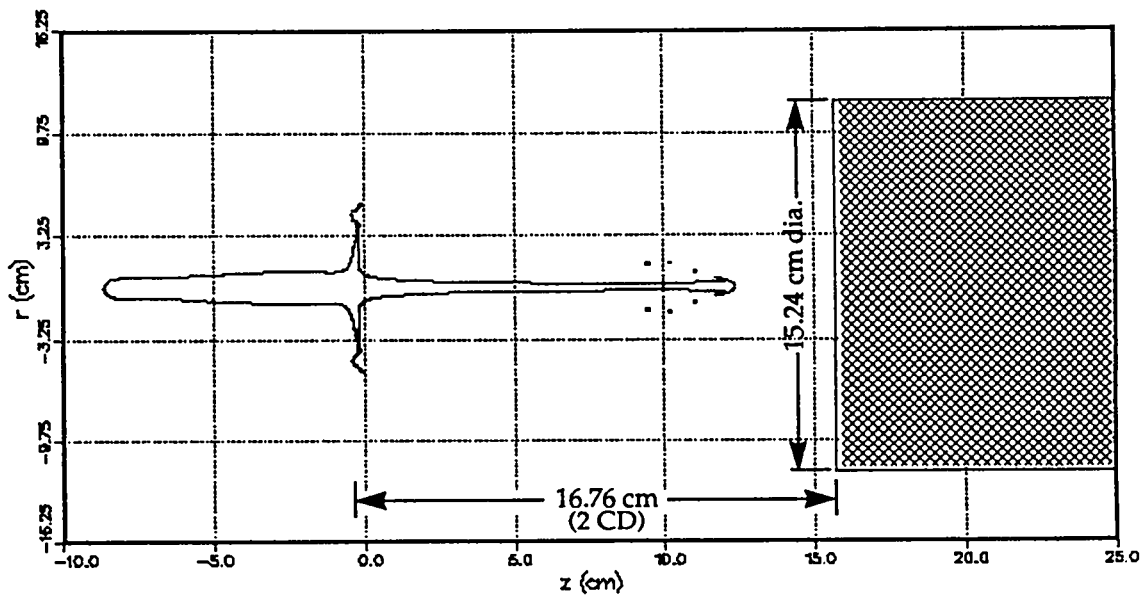

Fig. 11. View of the MESA-2D simulation after the steel target has been inserted into the calculation at 40 μs. The target is located two charge diameters (2 CD) from the base of the liner.

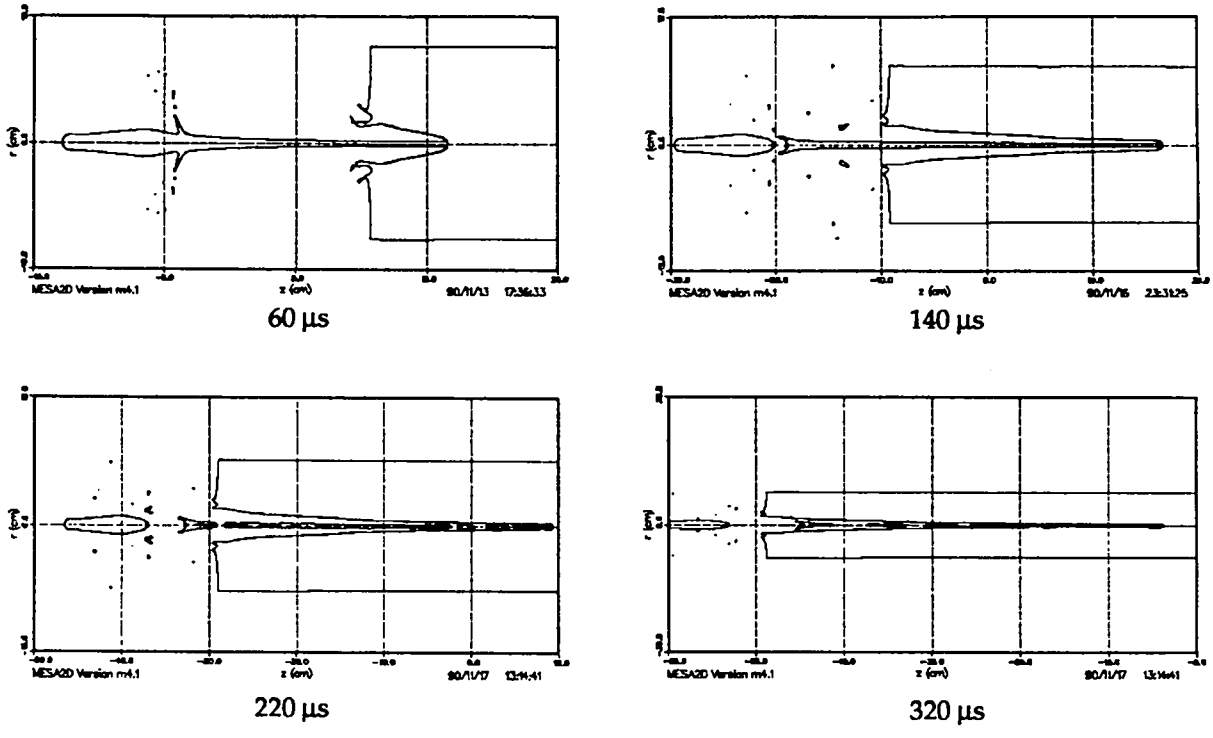

Fig. 12. Material interfaces for the MESA-2D jet penetration simulation. In this coordinate system, the billet is moving to the left at 0.3 cm/μs and the standoff is 2 CD.

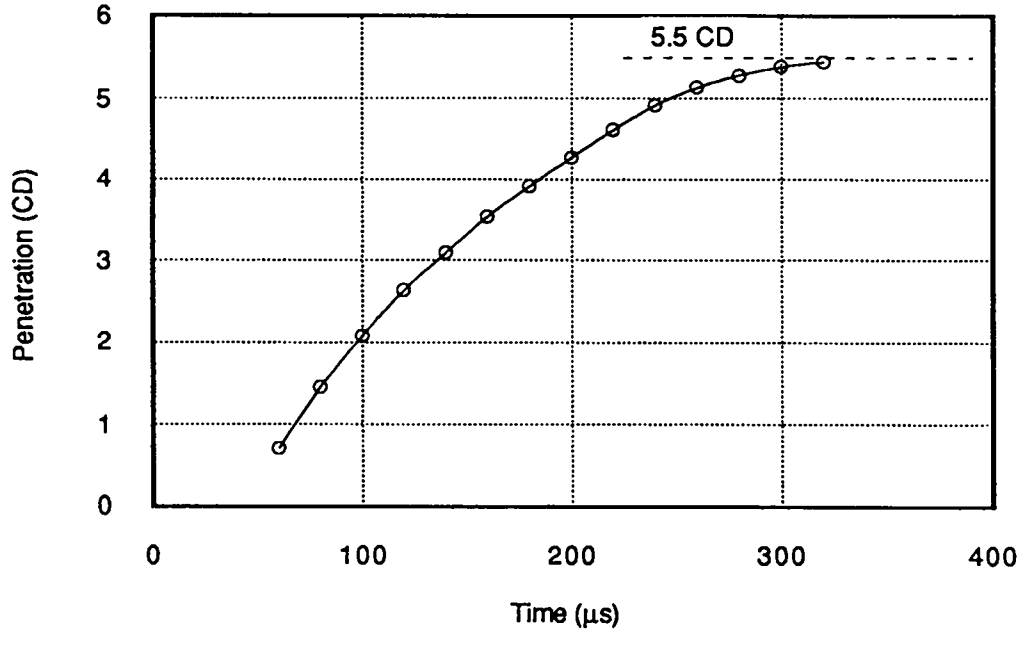

Fig. 13. Jet penetration into the target for the MESA simulation.

The computer prediction appears to overpredict the penetration by ~10% since it predicts a penetration of ~5.5 CD, and the largest penetration in the experiments was ~5 CD. We performed another simulation with the target yield strength lowered ~17% (Y = 9.2 kbar). The penetration for this case was nearly the same as that for the base case (< 3% change in penetration for 17% change in strength). It appears as though the predicted penetration is not very sensitive to the target yield strength. This result led us to believe that there is another more important mechanism controlling the penetration.

Analysis of the Jet Penetration Calculation

In the early stage of the penetration the jet is continuous whereas in the final stage (>~200μs) of the penetration process the jet has broken up into individual particles. Each succeeding particle that strikes the target has a smaller velocity than the one before it. The experiments[4] showed that the penetration is terminated while the jet particles are still striking the target. The minimum velocity particle (v_{min}) that causes additional penetration was measured, and it was found to be a function of both the target hardness and the standoff (v_{min} increases with both standoff and target hardness). For shots at 2 CD into 320 BHN armor, the measured value was v_{min} = 0.24 cm/μs. DiPersio et. al.[4] speculate that after the time that the particle velocity drops below v_{min}, the jet material starts sticking in the bottom of the crater rather than being carried out along the surface of the crater. This means that the succeeding particles strike jet material rather than target material and do not contribute to further penetration. Sectioned targets show that there is much jet material that has refilled the target hole.

We calculated the velocity of the particle striking the bottom of the crater at each dump time in the calculation, and this correlation is shown in Fig. 14. It indicates that indeed there is a change in the penetration mechanism at ~260 μs when v_{min} = 0.24 cm/μs and that particles that arrive later have a lower than expected velocity.

Detailed plots of the interfaces in the simulation were made to find the mechanism for the anomalous behavior of the particle velocity near 260 μs. Plots of the interfaces at each available dump time from 200 μs to 300 μs are shown in Fig. 15. With the aid of these plots we can easily see the sequence of events that lead to the sudden particle velocity decrease and eventually to the end of penetration. In Fig. 15, the jet particles are traveling to the right and impinging on the bottom of the crater. The following events are shown on the figure:

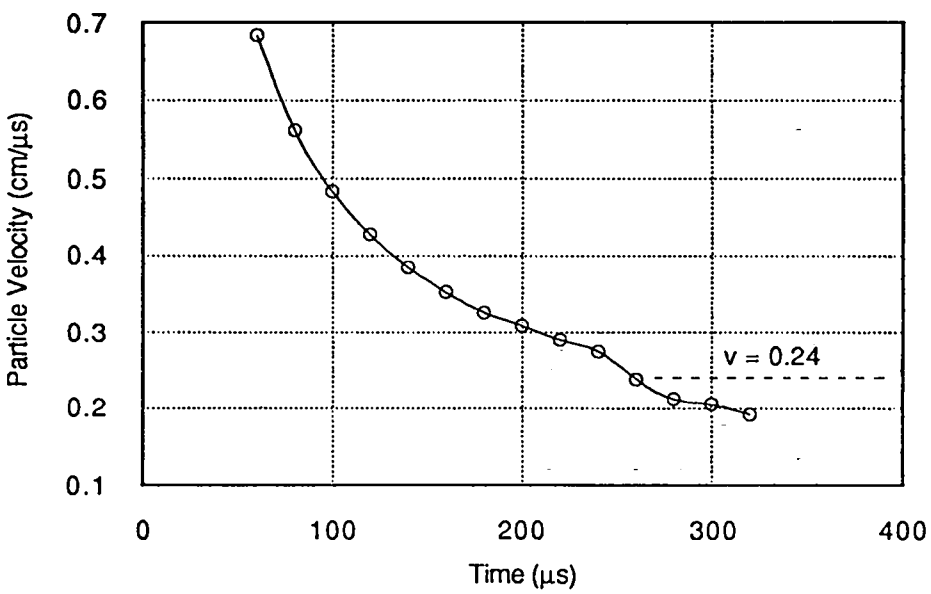

Fig. 14. Particle velocity for particle striking the bottom of the crater at each penetration.

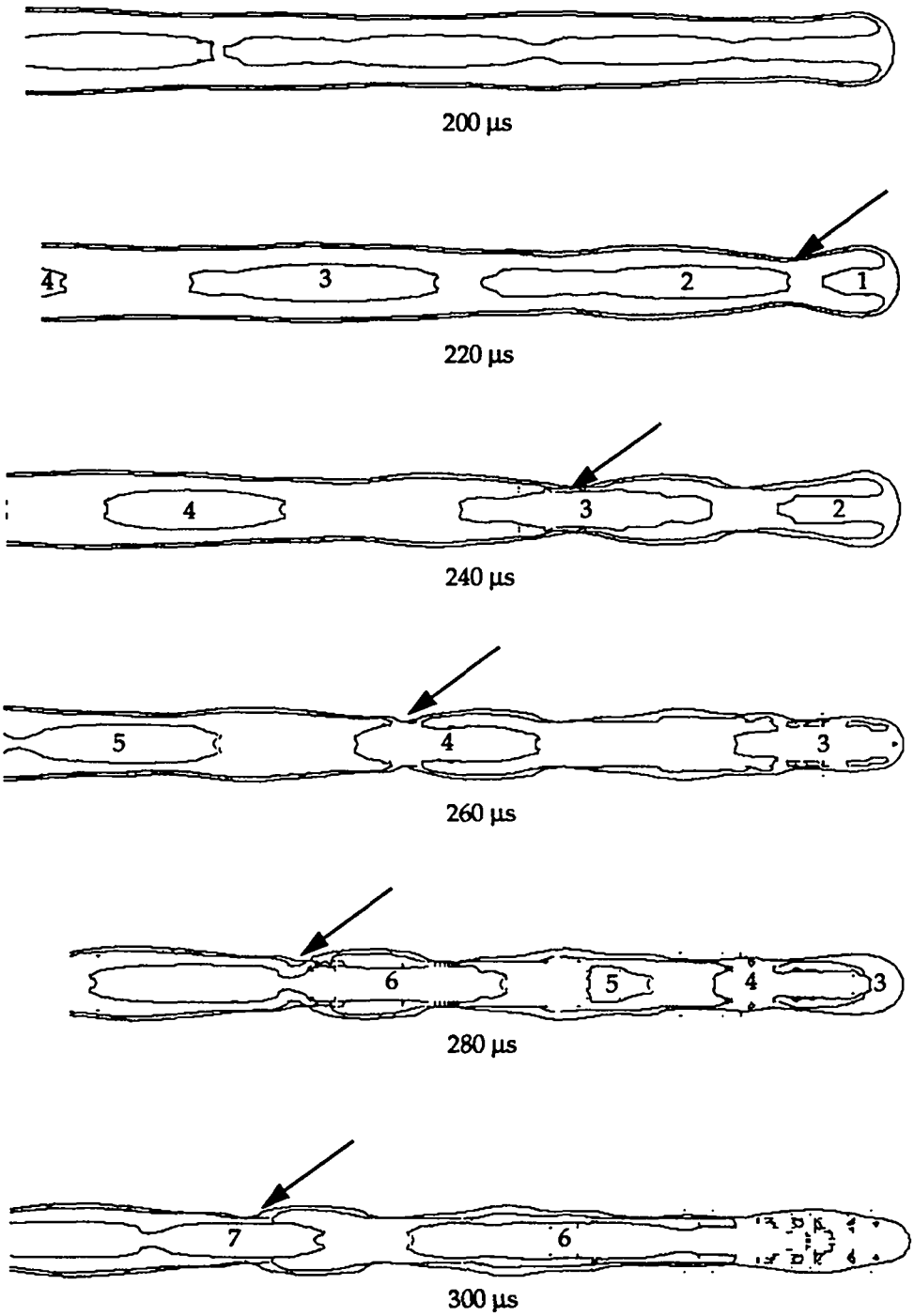

Fig. 15. Computer penetration prediction by a sequence of jet particles. The point where the crater first necks down and pinches off the jet particles is indicated by the arrow. The jet particles are numbered for identification between frames.

- At 200 μs, the crater is cylindrical and has a nearly uniform diameter near the bottom of the crater (the bottom 10 cm are shown on the figure). The jet is stretching and particulating. The jet material that has reached the bottom of the crater has coated the wall of the crater and is moving to the left and thus is not adding any debris to the bottom of the crater.

- At 220 μs, the front of the jet has particulated into slugs ~2-3 cm long. Slug-2 will reach the bottom of the crater and impact into fresh target material because slug-1 will be eroded by the time it arrives. An constriction in the crater surface is developing ~1 cm from the bottom of the crater. This point is indicated by an arrow on the figure.

- At 240 μs, the decrease in diameter of the crater wall leads to interference between the crater wall and slug-3. Its speed is slowing due to the contact with the crater wall. Jet material from the bottom of the crater does not erode onto the crater wall.

- At 260 μs, slug-3 has struck the bottom of the crater (but at a reduced velocity). The crater wall is severely interfering with slug-4. The back end of slug-4 will break off.

- At 280 μs, slug-4 is reaching the bottom of the crater before the remains of slug-3 could exit. Debris is starting to pile up in the bottom of the crater. Slug-5 has been broken off the tail of slug-4 and is slow moving with respect to those ahead and behind it. The crater surface is now interfering with slug-6.

- At 300 μs, slug-6 is running into debris left from those nearer the tip. More debris is piling up in the bottom of the crater, and the depth of the crater has almost stopped increasing.

The calculation predicts that the penetration will be stopped long before the jet material is used up. The mechanism is as speculated by DiPersio et. al.[4]; the penetration is stopped because jet material is not able to exit the crater, and succeeding particles impact the jet material debris rather than target material. The calculation provides some insight into the mechanism that terminates penetration. It predicts that the particulated material is interfered with by the crater walls so that the jet material cannot escape from the crater, and following particles reach the bottom of the crater at a reduced velocity from that expected if the interference had not occurred. This termination process may be sensitive to the strength of the jet and target.

The penetration mechanism is much more complicated than a one-dimensional eroding rod and appears to be at least two-dimensional in nature. The end of penetration is the result of a number of complicated mechanisms including the crater pinching off the jet, the jet particles breaking apart and slowing, and jet material not being able to exit from the crater. The total penetration as a function of the particle velocity impinging on the bottom of the crater is shown in Fig. 16. This figure shows the change in the penetration mechanism at v_{min} ~ 0.24 cm μs. We note that at this time, the predicted penetration is at the upper end of that measured experimentally (~4.7-4.9 CD) for "precision charges". This is as good as we can expect with the code calculation because the code is calculating the performance of a perfect jet and the actual jet can only achieve this as an upper limit.

SUMMARY

Our initial goal was to use the data from a standard shaped charge experiment as part of our QA of the MESA code. As our work progressed, we saw that a mesh and model sensitivity study would be useful in order to guide MESA users in modeling their own problems. We have thus provided this type of information in this report. It should be kept in mind that our conclusions may differ for other types of problems.

There were two different facets involved in this study: 1) jet formation from a shaped charge, and 2) jet penetration into a thick target. The code was assessed by its ability to perform and its accuracy in performing these types of calculations by comparing the code predictions with experimental data.

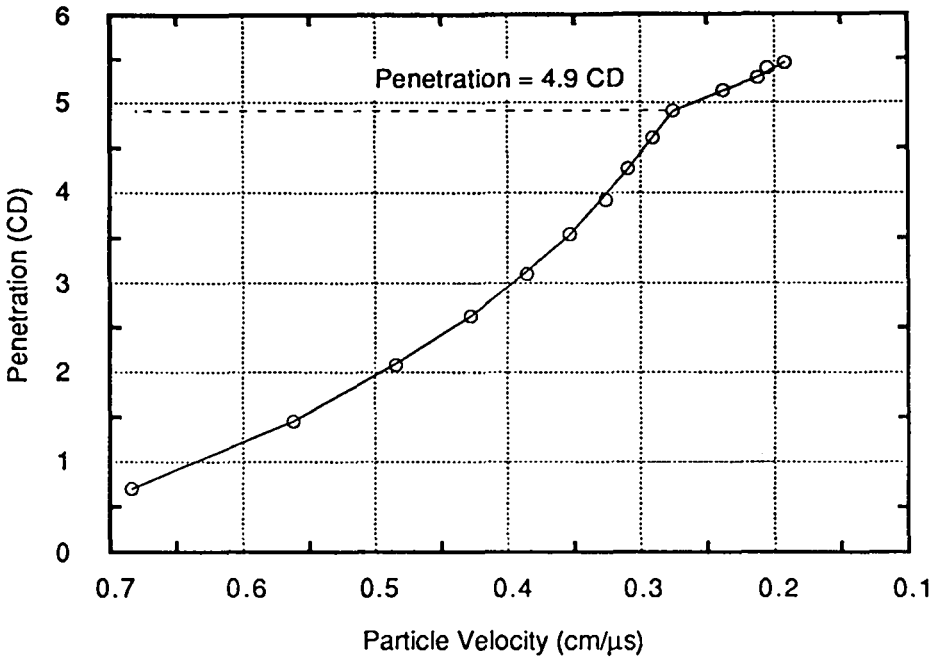

Fig. 16. Velocity of particle striking the bottom of the crater at each penetration depth.

Summary of Jet Formation Results

We used the jet tip speed as the figure of merit for comparisons of the calculations against experimental data. We found that both the MESA-2D and MESA-3D codes can accurately predict the jet tip speed. We found that the accuracy increases as the cell size decreases and that the predicted jet speed converges to the experimental measurement as the cell size decreases to zero.

We found that a variable mesh may be used in order to obtain results essentially equivalent to those from a uniform mesh simulation but using only 1/3 the computer resources. Likewise, we found that the use of a moving mesh in the simulation can decrease computer resources and increase accuracy.

We found it necessary to include material strength in the liner and that it is an important contributor to the calculated jet speed. The differences between the various strength models is small compared to the effect of neglecting strength in the liner. On the other hand, we found that it is not crucial to model either the charge case or the surrounding air for this particular charge. (This charge has an Aluminum case; charges with steel cases may be more sensitive to confinement). We found that small uncertainties in the JWL EOS constants have only a small effect on the predicted jet tip speed and thus; in this case, exact JWL constants are not critical to the predictions.

For the same noding configuration, we found that the 2D and 3D versions of the MESA code predict equivalent results and thus can be effectively combined in a design study. In this study, we were not able to run the 3D code with the small uniform sized cells used in the 2D simulations because of the large number of cells required, but when we employed a variable mesh which provides a cost effective calculation, the 3D code predicts approximately the correct jet tip speed. The 3D code needs ~10-15 times the number of cells and takes ~45-60 times the CPU for the same simulation as the 2D code. It does not appear practicable to model this problem with a cell size small enough to achieve mesh convergence with a 3D model. Because of this, we recommend a strategy that will make use of the capability of a 2-D model in conjunction with a 3D model. The 2D model could, for example, be used to perform a cell size sensitivity study and examine details of features in the problem using a zoning so fine that mesh convergence is achieved.

The 3D model is essential to gain an understanding of 3D features in the process being simulated and may be used to study, e.g., overall trends and 3-D geometry effects.

For all the parametric variations that we performed, the cell size effect is the most important consideration in setting up and modeling this problem. The size of the mesh cells should be given careful consideration when setting up a new geometry. A balance must be achieved between a large cell size that will give misleading information, and a cell size that will result in unreasonable computer costs. In this study we have shown how the user can employ a Galilean transformation and a variable mesh to increase accuracy and decrease computer costs.

Summary of Jet Penetration Results

The MESA codes are a valuable tool in explaining the penetration of a shaped charge into a target. The penetration of an "ideal" shaped charge was predicted to be about 10 percent greater than the measured value and the differences are explained by the variability of the experiments and by the penetration mechanism. It appears as though the predicted penetration is not only sensitive to the target yield strength but that there is some other important mechanism controlling the penetration depth.

The penetration mechanism is much more complicated than a one-dimensional eroding rod and appears to be at least two-dimensional in nature. The end of penetration is the result of a number of complicated mechanisms including the crater pinching off the jet, the jet particles breaking apart and slowing, and jet material not being able to erode onto the crater wall.

ACKNOWLEDGMENTS

The authors would like to thank Robert Karpp for discussions which were helpful in clarifying our understanding of the jet penetration process. We also grateful for the many suggestions and editorial assistance provided by Pat Mendius.

REFERENCES

1. J. D. Immele, Chairman, "Report of the Review Committee on Code Development and Material Modeling," Los Alamos National Laboratory report LA-UR-89-3416 (October 1989).

2. C. E. Anderson, "An Overview of the Theory of Hydrocodes," Int. J. Impact Engng, 5, pp. 33-59 (1987).

3. W. P. Walters and J. A. Zukas, Fundamentals of Shaped Charges, (John Wiley & Sons, 1989) pp. 178-180.

4. Robert DiPersio, Julius Simon, and Alfred B. Merendino, "Penetration of Shaped- Charge Jets into Metallic Targets," Ballistic Research Laboratories report No. 1296, (September, 1965).

5. D. L. Youngs, "Time Dependent Multi-Material Flow With Large Fluid Distortion," in K W. Morton and J. H. Baines, ed., Numerical Methods for Fluid Dynamics, Academic Press (1982).

6. Bram Van Leer, "Towards the Ultimate Conservative Difference Scheme. A Second- Order Sequel to Godunov's Method," J. of Comp. Phy., 32, pp. 101-136 (1979).

7. D. L. Youngs, "An Interface Tracking Method for a 3-D Eulerian Hydrodynamics Code," UK Atomic Weapons Establishment, AWRE/44/92/35 (1987).

8. D. J. Steinberg, S. G. Cochran, and M. W. Guinan, "A Constitutive Model for Metals Applicable at High-Strain Rate," J. Appl. Phy. 51, No. 3, pp. 1498-1504 (1980).

9. D. J. Steinberg and C. M. Lund, "A Constitutive Model For Strain Rates From 10-4 to 106 s-1," Journal de Physique, Colloque C3, Supplement au no9, Tome 49, (Septembre 1988).

10. G. R. Johnson and W. H. Cook, "A Constitutive Model and Data for Metals Subjected to Large Strains, High Strain Rates and High Temperatures," Seventh International Symposium on Ballistics, The Hague, The Netherlands (1983).

11. Paul S. Follansbee and U. F. Kocks, "A Constitutive Description of the Deformation of Copper Based on the Use of Mechanical Threshold Stress as an Internal State Variable," Acta metall. 36, No. 1, pp. 81-93 (1988).

12. J. N. Johnson, "Dynamic Fracture and Spallation in Ductile Solids," J. App. Phy. 52 (4) pp. 2812-2825 (1981).

13. G. R. Johnson and W. H. Cook, "Fracture Characteristics of Three Metals Subjected to Various Strains, Strain Rates, Temperatures and Pressures," Engineering Fracture Mechanics, 21, No. 1, pp 31 48 (1985).

14. E. L. Lee, H. C. Hornig, and J. W. Kury "Adiabatic Expansion of High Explosive Detonation Products," Lawrence Livermore National laboratory report, UCRL-50422 (May, 1968).

15. Charles W.Cranfill, "EOSPAC: A Subroutine Package for Accessing the Los Alamos SESAME EOS Data Library," Los Alamos National Laboratory report, LA-9728-M (August, 1983).

16. Charles L. Mader, Numerical Modeling of Detonations (University of California Press, Berkeley, 1979), pg. 56.

17. Dave Collins, "FRAC-IN-THE-BOX DOCUMENTATION," Los Alamos National Laboratory memo, X-6:DGC-88-40 (February, 1991).

18. M. Berger, "Detonation of High Explosives in Lagrangian Hydrodynamic Codes Using the Programmed Burn Technique," Los Alamos National Laboratory Report LA-6097-MS (December, 1975).

19. L. Penn, F. Helm, M. Finger, and E. Lee, "Determination of Equation-Of-State Parameters For Four Types of Explosive," Lawrence Livermore National Laboratory Report UCRL-51892 (August, 1975).

20. W. A. Bailey, R. A. Belcher, D. K. Chivers, and G. Eden, "Explosive Equation of State Determination by the AWRE Method," Proceedings of the Seventh Symposium (International) on Detonation, Naval Surface Weapons Center, Annapolis, Maryland (June, 1981).

21. Martin N. Raftenberg and Glenn Randers-Pehrson, "Modeling Electromagnetic Energy Coupling Effects in a Shaped-Charge Warhead," Ballistic Research Laboratory report BRL-TR-3278 (October 1991).

Appendix A

INPUT FILES FOR MESA-2D SIMULATION WITH STRENGTH AND A CONSTANT 0.5 mm UNIFORM CELL SIZE

GENERATOR Input

```
mesa2d (g)

Standard Charge Base Case-- Sesame EOS -- S-G Strength -- 1/2 mm mesh

 $probsize
          mcr = 120,    mcz = 840,
        mmats = 4,     mmix = 2700,    mcomp = 3,
     strength = .true.,              heburn = .true.,
 $end

 $options
       idgeom = 2,        idq = 1,
        ibcr1 = 0,      ibcr2 = 1, ibcz1 = 1, ibcz2 = 1,
     coordfac = 1.0e-4,
 $end

 $mesh
        ncellr =   120,
        ratior =   1.0,
        coordr =   0.0, 6.0,

        ncellz =   840,
        ratioz =   1.0,
        coordz = -17.0, 25.0,
 $end

 $mats
       mpri       = 3, 1, 2, 4,
       matbak     = 4,

       matname(1) = 4h3336,                          eosform(1) = 6hsesame,
            d0(1) = 8.93, e0(1) = 1.1622867732971e-3,    pmin(1) = -0.1,

       strform(1) = 3hs-g,      yld0(1) = 0.0012, yldmax(1) = 0.0064,
                                 sm0(1) = 0.477,   smmax(1) = 2.54,

      strcon(1,1) = 36.0, 0.0, 0.45, 0.0, 100., 2.8, 2.8,

       matname(2) = 8hAl  Case, eosform(2) = 4husup,
            d0(2) = 2.714, e0(2) = 0.0, pmin(2) = -0.1,
      eoscon(1,2) = 0.5392, 1.341, 0.0, 2.00,

      strcon(1,2) = 125., 0.0, 0.10, 0.0, 100., 6.5, 6.5,

       matname(3) = 8hOctol HE, eosform(3) = 3hjwl,
            d0(3) = 1.821, e0(3) = 0.0527, detvel(3) = 0.848,
      eoscon(1,3) = 0.38, 7.486, 8.19, 0.1338, 2.19,

       matname(4) = 8h    void, eosform(4) = 4hvoid,
            d0(4) = 0.0,
 $end

 $dets
       detz = -15.4, detr = 0.0, dett = 0.0,
 $end

          outer liner
```

```
$points
      rz =
  1,        4.36880,     -1.06426,
  2,        4.36880,     -1.27000,
  3,        4.19100,     -1.27000,
  4,    1.022027836,     -9.525454732,
  5,        0.00000,    -10.227875003,
$end

        inner liner
$points
      rz =
  6,        0.00000,    -10.022135003,
  7,    0.829952999,     -9.451724110,
  8,    4.049598816,     -1.06426,
$end

        outer case
$points
      rz =
  9,    4.54660,         0.0000,
 10,    4.54660,       -12.3190,
 11,    2.93370,       -16.5100,
 12,    0.00000,       -16.5100,
$end

        inner case
$points
      rz =
 13,    0.00000,       -15.4262,
 14,    2.54000,       -15.4262,
 15,    4.19100,       -11.1252,
 16,    4.36880,        -1.2700,
 17,    4.36880,         0.0000,
$end

      center of sphere

p points
      rz =
 18,    0.00000, -9.133135003,
$end

$curves
      circle =  4,  5,   7, 6,
      center = 18, 18,
      subdiv = 50, 50,
$end

        liner
$region
      mat = 1,
      pts = 1, 2, 3, 4, 5, 6, 7, 8,
$end

        case
$region
      mat = 2,
      pts = 9, 10, 11, 12, 13, 14, 15, 3, 16, 17,
$end

        he
$region
      mat = 3,
      pts = 3, 15, 14, 13, 5, 4,
```

```
$end
```

MESA Input

```
mesa2d (m)
0, 0.0, 0.0

$probsize
        mcomp    = 4,
        mmix     = 3000,
        strength = .true.,
        heburn   = .true.,
$end
$options
        actgrid = .true.,
        ibcr1 = 0, ibcr2 = 1, ibcz1 = 1, ibcz2 = 1,
        idq = 1,
        dt0 = 5.e-1, dtmin = 1.e-4, dtmax = 5.e-1, dth = 5.e-1,
        growdth = 1.25, growdt0 = 1.05,
        safdtc = .5, safdtur = .5, safdtuz = .5, safdtd = .5,
        cutacc = 1.0e-9, cutvolf = 1.0e-5, cutd = 1.0e-6, cutpf = .001,
        cq1 = 0.0, cq2 = 2.0,
        mlagcyc = 4,
        zap = .true.,
$end
$ops
        ropt = 0.0,  50.0,   ropdt = 10.0,
        mropsp = 1, 1,  mroplp = 0, 0,  mropdmp = 1, 1
$end
```

Appendix B

INPUT FILES FOR MESA-3D SIMULATION WITH STRENGTH AND A 1.1 FACTOR VARIABLE MESH SIZE

FRAC-IN-THE-BOX Input

```
!     outer liner
tabsf 1 c x 0.0 0.0 0.0
-10.227875003,    0.000000000
-10.227557482,    0.026364858
-10.226605102,    0.052714423
-10.225018416,    0.079033410
-10.222798345,    0.105306549
-10.219946176,    0.131518603
-10.216463563,    0.157654364
-10.212352528,    0.183698672
-10.207615454,    0.209636419
-10.202255090,    0.235452559
-10.196274545,    0.261132117
-10.189677288,    0.286660196
-10.182467146,    0.312021987
-10.174648303,    0.337202779
-10.166225292,    0.362187965
-10.157203001,    0.386963050
-10.147586664,    0.411513664
-10.137381857,    0.435825565
-10.126594502,    0.459884650
-10.115230855,    0.483676963
-10.103297509,    0.507188701
-10.090801386,    0.530406227
-10.077749735,    0.553316072
-10.064150126,    0.575904947
-10.050010450,    0.598159747
-10.035338907,    0.620067564
-10.020144009,    0.641615688
-10.004434570,    0.662791621
 -9.988219703,    0.683583078
 -9.971508813,    0.703977998
 -9.954311596,    0.723964551
 -9.936638025,    0.743531143
 -9.918498355,    0.762666423
 -9.899903106,    0.781359292
 -9.880863067,    0.799598906
 -9.861389282,    0.817374684
 -9.841493047,    0.834676314
 -9.821185903,    0.851493762
 -9.800479632,    0.867817270
 -9.779386244,    0.883637370
 -9.757917974,    0.898944885
 -9.736087278,    0.913730935
 -9.713906817,    0.927986944
 -9.691389459,    0.941704640
 -9.668548266,    0.954876068
 -9.645396488,    0.967493586
 -9.621947554,    0.979549875
 -9.598215068,    0.991037941
 -9.574212795,    1.001951121
 -9.549954659,    1.012283084
 -9.525454732,    1.022027836
 -1.27            4.191
 -1.27            4.3688
  0.0             4.3688
```

```
end
!     inner liner
tabsf 2 c x 0.0 0.0 0.0
-10.022135003,    0.000000000
-10.021877155,    0.021409978
-10.021103761,    0.042807536
-10.019815269,    0.064180263
-10.018012427,    0.085515759
-10.015696280,    0.106801649
-10.012868172,    0.128025585
-10.009529745,    0.149175256
-10.005682933,    0.170238391
-10.001329969,    0.191202774
 -9.996473378,    0.212056244
 -9.991115977,    0.232786702
 -9.985260874,    0.253382124
 -9.978911464,    0.273830563
 -9.972071433,    0.294120157
 -9.964744746,    0.314239136
 -9.956935655,    0.334175829
 -9.948648690,    0.353918672
 -9.939888657,    0.373456212
 -9.930660637,    0.392777116
 -9.920969985,    0.411870175
 -9.910822321,    0.430724314
 -9.900223532,    0.449328597
 -9.889179767,    0.467672230
 -9.877697431,    0.485744574
 -9.865783185,    0.503535144
 -9.853443940,    0.521033621
 -9.840686855,    0.538229854
 -9.827519330,    0.555113868
 -9.813949002,    0.571675869
 -9.799983744,    0.587906248
 -9.785631657,    0.603795592
 -9.770901066,    0.619334683
 -9.755800516,    0.634514506
 -9.740338767,    0.649326257
 -9.724524788,    0.663761344
 -9.708367753,    0.677811392
 -9.691877033,    0.691468252
 -9.675062196,    0.704724001
 -9.657932994,    0.717570950
 -9.640499365,    0.730001647
 -9.622771421,    0.742008880
 -9.604759446,    0.753585685
 -9.586473889,    0.764725346
 -9.567925356,    0.775421401
 -9.549124608,    0.785667645
 -9.530082550,    0.795458135
 -9.510810229,    0.804787191
 -9.491318825,    0.813649402
 -9.471619642,    0.822039627
 -9.451724110,    0.829952999
 -1.06426         4.049598816
 -1.06426         4.3688
  0.0             4.3688
end
!     outer case
tabsf 3 c x 0.0 0.0 0.0
   0.000,         4.5466
 -12.319,         4.5466
 -16.510,         2.9337
 -16.510,         0.0000
end
```

```
!     inner case
tabsf 4 c x 0.0 0.0 0.0
 -15.4262,        0.0000
 -15.4262,        2.5400
 -11.1252,        4.1910
  -1.2700,        4.1910
  -1.2700,        4.3688
   0.0000,        4.3688
 end
!
qcell 1 1 1.0 1 liner 1 -2
qcell 2 2 1.0 1 case  3 -4
qcell 3 3 1.0 1 he    4 -1
!
mesh x  1 -1.70000e+01
  420  2.50000e+01  1.00000000e+00
mesh y  1  0.00000e+00
   20  6.00000e+00  1.10408364e+00
mesh z  1  0.00000e+00
   20  6.00000e+00  1.10408364e+00
!     accuracy
ver .005
```

GENERATOR Input

```
mesa (g)
 Std Chrg -- 0.081" Liner -- Sesame -- S-G -- Var mesh
p$probsize
        heburn = .true.,
      strength = .true.
 $end
 $options
      ibc = 1, 1, 0, 1, 0, 1,
 $end
 $eos
      mpri = 3, 1, 2, 4,

        matnam(1) = 8hliner-Cu, eosform(1) = 8hsesame  ,
          rho0(1) = 8.93, sie0(1) = 1.1622867732971e-3, prsmin(1) = -0.1,
      ieoscon(1,1) = 3336,

      strmodel(1) = 8hs-g     ,yld0(1) = 0.0012, yldmax(1) = 0.0064,
                                 sm0(1) = 0.477,   smmax(1) = 2.54,

      strcon(1,1) = 36.0, 0.0, 0.45, 0.0, 100., 2.8, 2.8,

        matnam(2) = 8hAl  Case, eosform(2) = 8husup    ,
          rho0(2) = 2.714, sie0(2) = 0.0, prsmin(2) = -0.1,
      eoscon(1,2) = 0.5392, 1.341 , 0.0, 2.00,

      strcon(1,2) = 125., 0.0, 0.10, 0.0, 100., 6.5, 6.5,

        matnam(3) = 8hOctol HE, eosform(3) = 8hjwl     ,
          rho0(3) = 1.821, sie0(3) = 0.0527, detvel(3) = 0.848,
      eoscon(1,3) = 0.38, 7.486, 8.19, 0.1338, 2.19,

        matnam(4) = 8h    void, eosform(4) = 8hvoid      ,
          rho0(4) = 0.0,

 $end
 $dets
       hex = -15.4, hey = 0.0, hez = 0.0, het = 0.0
 $end
```

MESA-3D Input

```
mesa (m)
 0, 0.0, 0.0
Std Chrg - 0.081" Liner - Sesame - Variable Mesh
p$probsize
          mmix = 50000,
      strength = .true.,   heburn=.true.,
          iris = .false.,
 $end

 $options
         ibc = 1, 1, 0, 1, 0, 1,
      initsp = .true., initgd = .true., initlp = .true.,
      dtinit = .1, dtmin = .001,  dtmax = 1.0,
        mlag =  4, idartvis = 2, cutvof = 1.0e-4,  clean=.true.,
 $end

 $eos
      mpri = 2, 3, 1, 4,  cfrho(1)=.8, cfrho(2)=.8,
 $end

 $ops
      ropt = 0.0, 50.0, ropdt =  5.0,
      mropsp = 1, mroplp = 1, mropdmp = 1,
 $end
```

Page Range	NTIS Price Code	Page Range	NTIS Price Code	Page Range	NTIS Price Code	Page Range	NTIS Price Code
001–025	A02	151–175	A08	301–325	A14	451–475	A20
026–050	A03	176–200	A09	326–350	A15	476–500	A21
051–075	A04	201–225	A10	351–375	A16	501–525	A22
076–100	A05	226–250	A11	376–400	A17	526–550	A23
101–125	A06	251–275	A12	401–425	A18	551–575	A24
126–150	A07	276–300	A13	426–450	A19	576–600	A25
						601-up*	A99

*Contact NTIS for a price quote.

Los Alamos National Laboratory
Los Alamos,New Mexico 87545